Entanglement-Enhanced Quantum Metrology in Colored Noise by Quantum Zeno Effect

Xinyue Long,[1,*] Wan-Ting He,[2,*] Na-Na Zhang◉,[3,2,*] Kai Tang,[1] Zidong Lin,[1]
Hongfeng Liu,[1] Xinfang Nie,[1,4] Guanru Feng,[5] Jun Li,[1,4] Tao Xin,[1,4]
Qing Ai◉,[2,†] and Dawei Lu◉[1,4,‡]

[1]*Shenzhen Institute for Quantum Science and Engineering and Department of Physics,
Southern University of Science and Technology, Shenzhen 518055, China*
[2]*Department of Physics, Applied Optics Beijing Area Major Laboratory, Beijing Normal University, Beijing 100875, China*
[3]*School of Optoelectronic Engineering, Chongqing University of Posts and Telecommunications, Chongqing 400065, China*
[4]*Guangdong Provincial Key Laboratory of Quantum Science and Engineering, Southern University of Science and Technology,
Shenzhen 518055, China*
[5]*Shenzhen SpinQ Technology Company, Limited, Shenzhen, China*

In open quantum systems, the precision of metrology inevitably suffers from the noise. In Markovian open quantum dynamics, the precision can not be improved by using entangled probes although the measurement time is effectively shortened. However, it was predicted over one decade ago that in a non-Markovian one, the error can be significantly reduced by the quantum Zeno effect (QZE) [Chin, Huelga, and Plenio, Phys. Rev. Lett. **109,** 233601 (2012)]. In this work, we apply a recently developed quantum simulation approach to experimentally verify that entangled probes can improve the precision of metrology by the QZE. Up to $n = 7$ qubits, we demonstrate that the precision has been improved by a factor of $n^{1/4}$, which is consistent with the theoretical prediction. Our quantum simulation approach may provide an intriguing platform for experimental verification of various quantum metrology schemes.

Introduction.—Quantum metrology utilizes quantum entanglement and coherence to enhance the measurement precision over classical metrology [1–3]. In the absence of noise, the precision of classical metrology scales as $n^{-1/2}$, which is limited by the central-limit theorem with n being the number of resources implemented in the measurements. In contrast, quantum metrology can reach the Heisenberg limit, scaling as n^{-1}. However, in practice, any quantum system is inevitably subject to decoherence which results from interaction with the environment [4]. Because of decoherence, there will be no improvement in the measurement precision over classical metrology, although the measurement time may be effectively shortened [5]. In order to overcome this shortcoming, various methods have been put forward, e.g., squeezing [6], purification [7], and one-way quantum-computing-based teleportation [8]. It was shown that, instead of maximally entangled states, partially entangled initial states may reduce the error to some extent [5]. When the system interacts with a specific bath with a band structure, ideal precision may be retrieved as a result of the existence of the bound state [9,10]. When there is a correlation between the baths for individual qubits, an auxiliary qubit can be introduced to reach the Heisenberg limit [11–13]. Interestingly, the nonlinear interaction between the system and the physical quantity to be measured is used to surpass the Heisenberg limit [14–18]. However, the nonlinear interaction may not be easily realized in practical measurements.

Then, a question naturally comes to our minds: Can we figure out some practical method to improve the measurement precision in the presence of noise? It is shown that there are, generally, three stages in open quantum dynamics, including the well-known exponential decay in the intermediate stage [19]. However, in the first stage, the open quantum system decays in a Gaussian way, where the quantum Zeno effect (QZE) [20–26] happens. It has been pointed out that due to the QZE, metrology using maximally entangled states is superior to the one using product states by a factor of $n^{1/4}$ [27,28]. On the other hand, recently, we have theoretically proposed and experimentally demonstrated in a nuclear magnetic resonance (NMR) platform, to simulate the quantum dynamics for various Hamiltonians and spectral densities [29–31]. In these works, the bath-engineering technique [32–35] enables a theoretically exact, fully controllable, and practically efficient quantum simulation [36,37] approach. Using the approach, we show that the non-Markovianity of the open quantum dynamics should essentially be characterized from both aspects of global and local points of view, e.g., quantum mutual information vs quantum Fisher information flows [31,38–40]. It is this theoretically exact and fully controllable characteristic that enables us to experimentally verify the quantum metrology scheme proposed in Refs. [27,28], which requires homogeneity of the qubits.

Protocol.—The bath-engineering technique offers a way to engineer arbitrary environments by modulating the control field [32,33]. By applying a time-dependent magnetic field to the total system, we can artificially add a spectral characteristic noise, so as to simulate an arbitrary noisy environment. The Hamiltonian of the total system can be written as $H(t) = H_S + H_{SB}(t)$, where $H_S = \sum_m \varepsilon_m |m\rangle\langle m| + \sum_{m \neq n} J_{mn} |m\rangle\langle n|$ is the system Hamiltonian, and $H_{SB}(t)$ is the noise Hamiltonian to simulate the system-bath (SB) couplings. When simulating the pure-dephasing noise, cf. Fig. 1(a), the noise Hamiltonian is $H_{SB}(t) = \sum_m \beta_m(t) |m\rangle\langle m|$. $\beta_m(t)$'s are stochastic errors generated by performing amplitude and phase modulations on a carrier [29,30]

$$\beta_m(t) = \alpha_z \sum_{j=1}^{J} \omega_j F(\omega_j) \cos(\omega_j t + \psi_j^{(m)}), \quad (1)$$

where α_z is the amplitude of the dephasing noise, ω_b ($J\omega_b$) is the base (cutoff) frequency with $\omega_j = j\omega_b$, $F(\omega_j)$ is the modulation function of a specific spectral characteristic noise, and $\psi_j^{(m)}$'s are a set of random numbers. For a noise of Gaussian type, the average over the ensemble is equivalent to the average over the time [41]. The
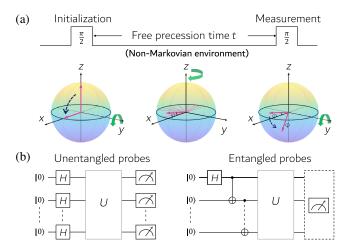

FIG. 1. (a) Single-qubit Ramsey experiment for quantum metrology under non-Markovian noise. The free precession is governed by non-Markovian dynamics, which can be simulated using the ensemble-averaging technique. This averaging can be visualized in the Bloch sphere: A large number of identical initial probes undergo phase diffusion owing to their different modulated Hamiltonians, leading to an attenuation in amplitude for the overall spin signal. This attenuation gives rise to the error in quantum-metrology experiments. (b) Quantum circuits for multi-qubit Ramsey experiment under non-Markovian noise with unentangled and entangled probes, respectively. The evolution U is the simulation of non-Markovian dynamics. For the case of entangled probes, the readout is typically some collective measurement [5,6].

ensemble-averaged decoherence factor reads $\Gamma(t) = \alpha_z^2 \sum_{j=1}^{J} F(\omega_j)^2 \sin^2(\omega_j t/2)$, as determined by the power spectral density of the noise, which is the Fourier transform of the second-order correlation function $\langle \beta_m(t+\tau)\beta_m(t) \rangle$ [32,33].

We consider a system Hamiltonian $H_S = \sum_{k=1}^{n} \omega_0 \sigma_k^z/2$, which is subject to a pure-dephasing noise [27]. We present an illustration for the case with a single qubit in Fig. 1(a). Initially, the qubit is prepared at $(|0\rangle + |1\rangle)/\sqrt{2}$. Afterwards, it unitarily evolves at the equator of the Bloch sphere with rate $\omega_0 + \beta_1(t)$. In order to mimic the pure dephasing, we generate a large number of realizations with the same initial state and obtain the final result by averaging over the random ensemble with a different rate $\beta_1(t)$ after a second $\pi/2$ pulse. We assume a Drude-Lorentz spectral density, i.e., $J_k(\omega) = J(\omega) = 2\lambda\gamma\omega/(\omega^2 + \gamma^2)$, where λ is the reorganization energy and γ is the relaxation rate. A generic spectral density can be decomposed into a summation of Lorentzian forms. The modulation function then becomes $F(\omega_j) = [\lambda\gamma\omega_0 \coth(\beta\omega_j)/(\omega_j^3 + \gamma^2\omega_j)]^{1/2}$. The quantum dynamics of the system is exactly described by the time-local master equation [4,42]

$$\frac{\partial}{\partial t}\rho(t) = -i[H_S, \rho] + \sum_k \gamma_k(t)(\sigma_k^z \rho \sigma_k^z - \rho). \quad (2)$$

Note that $\gamma_k(t)$ is explicitly dependent on time. According to the bath-engineering technique, the ensemble-averaged decoherence rate is $\gamma_k(t) = (\alpha_z^2/2) \sum_{j=1}^{J} \omega_j F(\omega_j)^2 \sin(\omega_j t)$.

In Fig. 1(b), we present the quantum circuit for the quantum metrology scheme for the product and entangled states, respectively. For the former case, the probes are prepared at $[(|0\rangle + |1\rangle)/\sqrt{2}]^{\otimes n}$ and then evolve under the unitary evolution $U = \exp(-i \int_0^t d\tau [H_S + \sum_k \beta_k(\tau)\sigma_k^z])$, which will not induce entanglement between different qubits but mimic the noise. Then, we perform the individual measurements on each qubit, respectively, since all qubits are disentangled. However, for the latter case, since the probes are initialized at the maximally entangled state $(|0\rangle^{\otimes n} + |1\rangle^{\otimes n})/\sqrt{2}$, we only perform a collective measurement after the same U. For open quantum dynamics governed by the master equation (2), the variances of the measured frequency for the unentangled and entangled probes are, respectively, $\delta\omega_0^2|_u = \exp[2\Gamma(t_u)]/(nTt_u)$ and $\delta\omega_0^2|_e = \exp[2n\Gamma(t_e)]/(n^2Tt_e)$, where $\Gamma(t) = \int_0^t \gamma_k(t')dt'$ is the decoherence factor for a single qubit, and the subscript $u(e)$ refers to the unentangled (entangled) state. The optimal times to perform the measurement are determined by $2t_u\gamma_k(t_u) = 1$ and $2nt_e\gamma_k(t_e) = 1$, respectively. When the decoherence rate $\gamma_k(t) = c$ is time independent, the variances $\delta\omega_0^2 = 2ce/(nT)$ for both initial states are the same, although the optimal times are different, i.e., $t_u = 1/(2c)$ vs $t_e = 1/(2nc)$. However, when the QZE occurs, i.e., $\gamma_k(t) = 2ct$, the variance for the unentangled probes is

(a)

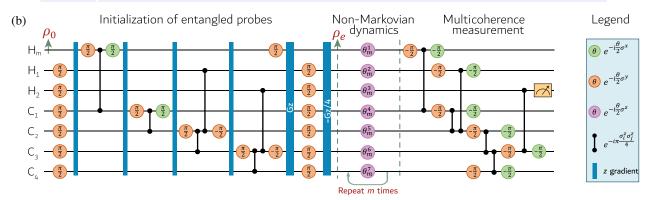|	H_m	H_1	H_2	C_1	C_2	C_3	C_4	T_1 (s)	T_2 (s)
H_m	1126.8							3.2	1.1
H_1	6.8	4188.1						5.2	1.1
H_2	-1.7	15.5	3511.2					5.3	1.0
C_1	127.2	3.9	6.3	2572.4				7.5	1.6
C_2	-7.1	155.6	-0.6	41.6	21925.0			7.9	1.5
C_3	6.6	-1.8	161.5	1.5	69.6	18478.2		8.7	1.6
C_4	-0.9	6.5	3.3	7.1	1.2	72.3	25279.0	19.1	1.2

(b)

FIG. 2. (a) Molecular structure and relevant parameters of the seven-qubit NMR processor. Chemical shifts (diagonal, Hz), scalar coupling strengths (off-diagonal, Hz), and relaxation times (T_1 and T_2) are all listed in the table. (b) Pulse sequence for the 7-qubit Ramsey experiment using the entangled probe under non-Markovian noise. To simulate the non-Markovian dynamics, the rotating angles θ_m^j are carefully designed by ensemble-averaging modulation. A step-by-step description of the sequence can be found in the SM [43].

inferior to that for the entangled ones, as $\delta\omega_0^2|_u = 2\sqrt{ce}/(nT) > \delta\omega_0^2|_e = 2\sqrt{nce}/(n^2T)$ with $t_u = (4c)^{-1/2} > t_e = (4nc)^{-1/2}$. Hereafter, we shall give an introduction to the experimental details.

Experiment.—The experiments are performed on a Bruker 600 MHz spectrometer at room temperature. The sample is ^{13}C-labeled trans-crotonic acid dissolved in d_6 acetone, which consists of three ^{1}H and four ^{13}C nuclear spins, forming a seven-qubit quantum processor. The molecular structure of the sample is shown in Fig. 2(a). The internal Hamiltonian of this system can be described as

$$\mathcal{H}_{\mathrm{NMR}} = -\sum_{i=1}^{7} \frac{\omega_i}{2}\sigma_i^z + \sum_{i<j,=1}^{7} \frac{\pi}{2}J_{ij}\sigma_i^z\sigma_j^z, \qquad (3)$$

where $\omega_i/2\pi$ is the Larmor frequency of the ith spin, and J_{ij} is the scalar coupling strength between spins i and j. The corresponding parameters are listed in Fig. 2(a), as well as the relaxation times T_1 and T_2.

Overall, the experiment aims to observe the enhancement of quantum metrology with entangled probes under the non-Markovian circumstance. This is demonstrated using the Ramsey magnetometry, which typically contains three major stages: (i) preparation of initial probe states, (ii) accumulation of an energy-splitting dependent phase,

and (iii) measurement of that phase. In the following, we will describe each stage in detail.

(i) Prepare the two types of probe states: the unentangled probe $|\psi_0\rangle_u = [(|0\rangle + |1\rangle)/\sqrt{2}]^{\otimes n}$, and the maximally entangled probe $|\psi_0\rangle_e = (|0\rangle^{\otimes n} + |1\rangle^{\otimes n})/\sqrt{2}$. For the unentangled probe, the processor is initialized to the pseudopure state $|0\rangle^{\otimes n}$ (up to an identity matrix) from the thermal equilibrium state ρ_0 using the cat-state method [45]. Followed by a 2-ms-shaped pulse to perform a collective single-qubit rotation $R_y(\pi/2)$ on all qubits, the system is prepared into $|\psi_0\rangle_u$ with over 99% fidelity. The pulse sequence can be found in the Supplemental Material (SM) [43].

For the entangled probe, we directly start from the thermal equilibrium ρ_0, and eventually prepare the state $\rho_e = |0\rangle^{\otimes n}\langle 1| + |1\rangle^{\otimes n}\langle 0|$ with the aid of nearest-neighbor scalar couplings and gradient-echo techniques [43], as shown in Fig. 2(b). Despite it not being the exact form of $|\psi_0\rangle_e$, the dynamics of ρ_e for the quantum metrology purpose is the same since the frequency information is just encoded in the phase accumulation of coherent terms [43]. In addition, the creation of ρ_e avoids regular initialization of the pseudopure state, which reduces the sequence complexity remarkably.

(ii) For the target system $H_S = (\omega_0/2)\sum_{i=1}^{n}\sigma_i^z$ with ω_0 being the energy splitting to be measured, let the probes
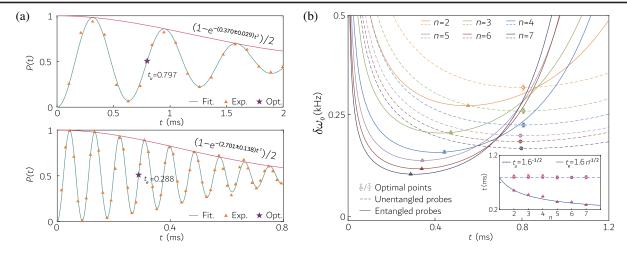
FIG. 3. (a) Dynamics of population $P(t)$ for the unentangled (top panel) and entangled (bottom panel) probes. Blue curves are obtained by numerically fitting the experimental data (yellow triangles) using Eq. (4), and red lines are envelopes with the form $(1 - e^{-\Gamma(t)})/2$, which depicts the time-dependent decoherence factor $\Gamma(t)$. The star symbol represents the optimal measurement point determined by the experiment. (b) Standard deviation $\delta\omega_0$ of the measured frequency with respect to the variation of t. Dashed (solid) curves are fitting results corresponding to the unentangled (entangled) probes for different numbers of qubits. Triangles and dots are the optimal measurement points. The scaling behavior of these optimal times when changing n is shown in the inset.

precess unperturbed for a duration t under the non-Markovian noise. This non-Markovian circumstance is simulated by the aforementioned bath-engineering technique. Explicitly, we introduce an additional time-dependent Hamiltonian term in the form of $H_{\mathrm{SB}}^m(t) = \sum_{i=1}^{n} \beta_i^m(t)\sigma_i^z$, where $\beta_i^m(t)$'s are stochastic errors subject to Drude-Lorentz spectral density as shown in Eq. (1), and m is the sampling number so as to approximate the non-Markovian noise via the ensemble-averaging approach [43]. So the total Hamiltonian in the mth experiment can be written as $H_S + H_{\mathrm{SB}}^m(t)$. Note that the evolution of this Hamiltonian corresponds to a collective single-qubit rotation about the z axis, which can be easily implemented in most physical systems. In addition, this time-dependent Hamiltonian can be discretized into time-independent slices for experimental realization (here, we use 10^3 slices [43]). Regarding the experimental parameters, we set $\omega_0 = 10$ kHz and choose $m = 20$ samples for ensemble average, which can already approximate the non-Markovian environment with a high precision [43].

(iii) Read out the accumulated phase. For the unentangled probes, the final phase is encoded in each individual qubit, so the readout only involves single-qubit measurements, which is similar to the standard Ramsey interferometry experiment. For the entangled probes, the final phase is retained in the relative phase between $|00, \ldots, 0\rangle$ and $|11, \ldots, 1\rangle$, and we apply the multicoherence measurement technique [46] to extract that phase. As shown in Fig. 2(b), this technique involves a series of elementary quantum gates, which can be extended to other systems as well. Subsequently, the transition probabilities are computed by averaging over the ensemble with $m = 20$ samples to simulate the non-Markovian decay.

Results.—We have conducted Ramsey experiments for $n = 2 \sim 7$ qubits. Taking the seven-qubit case as an example, the transition probability $P(t)$ is shown in Fig. 3(a) for both the unentangled (top panel) and entangled (bottom panel) probes. Compared to the unentangled case, $P(t)$ in the entangled case manifests a much faster oscillation owing to the rapid accumulation (~ 7 times) of phase. We use the theoretical form

$$P(t) = \frac{1}{2}[1 - \cos(n\omega_0 t)e^{-n\Gamma(t)}], \tag{4}$$

to fit the experimental data which gives the energy-splitting frequency ω_0 and decoherence factor $\Gamma(t)$. For the unentangled probes, the measured frequency is $\omega_0|_u = 9.871$ kHz and the decoherence factor is $\Gamma_u = (0.370 \pm 0.029)t^2$. For the entangled probes, the measured frequency is $\omega_0|_e = 10.142$ kHz and the decoherence factor is $\Gamma_e = (2.701 \pm 0.138)t^2$. The minimum standard deviations of the frequencies are $\delta\omega_0|_u = 0.169 \pm 0.003$ kHz and $\delta\omega_0|_e = 0.105 \pm 0.001$ kHz at the optimal measurement times $t_u = 0.797 \pm 0.032$ ms and $t_e = 0.288 \pm 0.003$ ms, respectively. Hence, the ratio of the sensitivity enhancement is $r = \delta\omega_0|_u/\delta\omega_0|_e = 1.608 \pm 0.035 \approx 7^{\frac{1}{4}}$, indicating that the entangled probes are, indeed, superior to the unentangled ones under the non-Markovian environment. Note that the readout of the NMR experiment is from the ensemble average result, which means the statistical error by repeating experiments is almost negligible. So, in this work, the error bars represent experimental uncertainties by error propagation from the fitting uncertainties in Fig. 3(a); see SM for details [43].
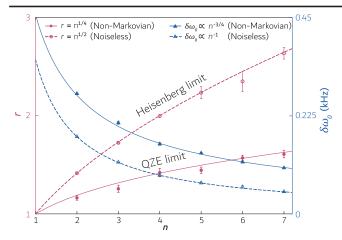
FIG. 4. Experimental results of the ratio $r = \delta\omega_0|_u / \delta\omega_0|_e$ (dots) and the minimum standard deviation $\delta\omega_0|_e$ (triangles) for different numbers of qubits n. Under the non-Markovian noise, the sensitivity is enhanced by $r = n^{1/4}$ (solid red curve) with the entangled probes, reaching the QZE limit; $\delta\omega_0|_e$ scales as $n^{-3/4}$ (solid blue curve). In the absence of noise, the sensitivity enhancement is governed by the Heisenberg limit $r = n^{1/2}$ (dashed red curve), and $\delta\omega_0|_e$ scales as n^{-1} (dashed blue curve).

For the other numbers of qubits, the experimentally measured frequencies ω_u and ω_e, in association with their respective decoherence factors Γ_u and Γ_e, can be found in SM [43]. The standard deviation of the estimated frequency is obtained by processing the experimental data, as shown in Fig. 3(b), where the dashed and solid lines are for the unentangled and entangled probes, respectively. For the unentangled probes, the optimal measurement time t_u is almost the same for different n's and the minimum standard deviation $\delta\omega_0|_u$ is proportional to $n^{-1/2}$. For the entangled probes, t_e and $\delta\omega_0|_e$ decrease with the growth of n. By varying the number of qubits, we compute the ratio $r = \delta\omega_0|_u / \delta\omega_0|_e$ to estimate the improvement of sensitivity with the entangled probes; see the solid red curve in Fig. 4. As predicted, the experimentally observed r scales as $r \sim n^{1/4}$, which is the QZE limit. For comparison, we have performed another group of experiments in the absence of noise [43]. In this noiseless scenario, the ratio of sensitivity r reaches the Heisenberg limit, scaling as $r \sim n^{1/2}$ by the dashed red curve in Fig. 4.

In addition, we depict distinct tendencies of the minimum standard deviation $\delta\omega_0|_e$ of the entangled probes for non-Markovian and noiseless environments, respectively. As shown in Fig. 4, with the growth in number of qubits, experimental results show that $\delta\omega_0|_e \propto n^{-3/4}$ for the non-Markovian noise by the solid blue curve, while $\delta\omega_0|_e \propto n^{-1}$ for the noiseless case by the dashed blue curve. Definitely, our high-precision experiment is sufficient to verify that the measurement accuracy of the entangled probes can reach the QZE limit under the non-Markovian noise.

Conclusion.—We experimentally demonstrate that the entangled probes can enhance the sensitivity of quantum metrology by the QZE. When the coherence decays quadratically with time, the entangled probes optimize the time for performing the measurement. On the contrary, when the decoherence rate is time independent, the entangled probes cannot effectively improve the precision but shorten the measurement time. We remark that, since our quantum simulation approach can subtly engineer the parameters of both the system and bath, it may provide an effective platform for experimentally verifying various quantum metrology schemes, e.g., achieving ideal precision by coupling to a bath with a band structure [9]. It can also be implemented in other physical systems [32,47].

*These authors contributed equally to this work.
†aiqing@bnu.edu.cn
‡ludw@sustech.edu.cn

[1] C. M. Caves, Quantum-mechanical noise in an interferometer, Phys. Rev. D **23**, 1693 (1981).
[2] V. Giovannetti, S. Lloyd, and L. Maccone, Quantum-enhanced measurements: Beating the standard quantum limit, Science **306**, 1330 (2004).
[3] L. Pezzè, A. Smerzi, M. K. Oberthaler, R. Schmied, and P. Treutlein, Quantum metrology with nonclassical states of atomic ensembles, Rev. Mod. Phys. **90**, 035005 (2018).
[4] H. P. Breuer and F. Petruccione, *The Theory of Open Quantum Systems* (Oxford University Press, New York, 2002).
[5] S. F. Huelga, C. Macchiavello, T. Pellizzari, A. K. Ekert, M. B. Plenio, and J. I. Cirac, Improvement of Frequency Standards with Quantum Entanglement, Phys. Rev. Lett. **79**, 3865 (1997).
[6] J. Ma, X. Wang, C. P. Sun, and F. Nori, Quantum spin squeezing, Phys. Rep. **509**, 89 (2011).

[7] K. Yamamoto, S. Endo, H. Hakoshima, Y. Matsuzaki, and Y. Tokunaga, Error-mitigated quantum metrology via virtual purification, arXiv:2112.01850.

[8] Y. Matsuzaki, S. Benjamin, S. Nakayama, S. Saito, and W. J. Munro, Quantum Metrology Beyond the Classical Limit Under the Effect of Dephasing, Phys. Rev. Lett. **120,** 140501 (2018).

[9] K. Bai, Z. Peng, H.-G. Luo, and J.-H. An, Retrieving Ideal Precision in Noisy Quantum Optical Metrology, Phys. Rev. Lett. **123,** 040402 (2019).

[10] Q. Ai and J.-Q. Liao, Quantum anti-Zeno effect in artificial quantum systems, Commun. Theor. Phys. **54,** 985 (2010).

[11] T. Monz, P. Schindler, J. T. Barreiro, M. Chwalla, D. Nigg, W. A. Coish, M. Harlander, W. Hänsel, M. Hennrich, and R. Blatt, 14-Qubit Entanglement: Creation and Coherence, Phys. Rev. Lett. **106,** 130506 (2011).

[12] W.-T. He, H.-Y. Guang, Z.-Y. Li, R.-Q. Deng, N.-N. Zhang, J.-X. Zhao, F.-G. Deng, and Q. Ai, Quantum metrology with one auxiliary particle in a correlated bath and its quantum simulation, Phys. Rev. A **104,** 062429 (2021).

[13] S. Kukita, Y. Matsuzaki, and Y. Kondo, Heisenberg-Limited Quantum Metrology Using Collective Dephasing, Phys. Rev. Applied **16,** 064026 (2021).

[14] S. Boixo, S. T. Flammia, C. M. Caves, and J. M. Geremia, Generalized Limits for Single-Parameter Quantum Estimation, Phys. Rev. Lett. **98,** 090401 (2007).

[15] X. Nie, J. Li, J. Cui, Z. Luo, J. Huang, H. Chen, C. Lee, X. Peng, and J. Du, Quantum simulation of interaction blockade in a two-site Bose–Hubbard system with solid quadrupolar crystal, New J. Phys. **17,** 053028 (2015).

[16] S. Choi and B. Sundaram, Bose-Einstein condensate as a nonlinear Ramsey interferometer operating beyond the Heisenberg limit, Phys. Rev. A **77,** 053613 (2008).

[17] S. M. Roy and S. L. Braunstein, Exponentially Enhanced Quantum Metrology, Phys. Rev. Lett. **100,** 220501 (2008).

[18] M. Napolitano, M. Koschorreck, B. Dubost, N. Behbood, R. J. Sewell, and M. W. Mitchell, Interaction-based quantum metrology showing scaling beyond the Heisenberg limit, Nature (London) **471,** 486 (2011).

[19] H. Nakazato, M. Namiki, and S. Pascazio, Temporal behavior of quantum mechanical systems, Int. J. Mod. Phys. B **10,** 247 (1996).

[20] Q. Ai, Y. Li, H. Zheng, and C. P. Sun, Quantum anti-Zeno effect without rotating wave approximation, Phys. Rev. A **81,** 042116 (2010).

[21] Q. Ai, D. Xu, S. Yi, A. G. Kofman, C. P. Sun, and F. Nori, Quantum anti-Zeno effect without wave function reduction, Sci. Rep. **3,** 1752 (2013).

[22] P. M. Harrington, J. T. Monroe, and K. W. Murch, Quantum Zeno Effects from Measurement Controlled Qubit-Bath Interactions, Phys. Rev. Lett. **118,** 240401 (2017).

[23] S. Virzì, A. Avella, F. Piacentini, M. Gramegna, T. Opatrný, A. G. Kofman, G. Kurizki, S. Gherardini, F. Caruso, I. P. Degiovanni, and M. Genovese, Quantum Zeno and Anti-Zeno Probes of Noise Correlations in Photon Polarization, Phys. Rev. Lett. **129,** 030401 (2022).

[24] A. H. Kiilerich and K. Mølmer, Quantum Zeno effect in parameter estimation, Phys. Rev. A **92,** 032124 (2015).

[25] H.-V. Do, C. Lovecchio, I. Mastroserio, N. Fabbri, F. S. Cataliotti, S. Gherardini, M. M. Müller, N. D. Pozza, and F. Caruso, Experimental proof of quantum Zeno-assisted noise sensing, New J. Phys. **21,** 113056 (2019).

[26] D. K. Burgarth, P. Facchi, V. Giovannetti, H. Nakazato, S. Pascazio, and K. Yuasa, Exponential rise of dynamical complexity in quantum computing through projections, Nat. Commun. **5,** 5173 (2014).

[27] A. W. Chin, S. F. Huelga, and M. B. Plenio, Quantum Metrology in Non-Markovian Environments, Phys. Rev. Lett. **109,** 233601 (2012).

[28] Y. Matsuzaki, S. C. Benjamin, and J. Fitzsimons, Magnetic field sensing beyond the standard quantum limit under the effect of decoherence, Phys. Rev. A **84,** 012103 (2011).

[29] B.-X. Wang, M.-J. Tao, Q. Ai, T. Xin, N. Lambert, D. Ruan, Y.-C. Cheng, F. Nori, F.-G. Deng, and G.-L. Long, Efficient quantum simulation of photosynthetic light harvesting, npj Quantum Inf. **4,** 52 (2018).

[30] N.-N. Zhang, M.-J. Tao, W.-T. He, X.-Y. Chen, X.-Y. Kong, F.-G. Deng, N. Lambert, and Q. Ai, Efficient quantum simulation of open quantum dynamics at various Hamiltonians and spectral densities, Front. Phys. **16,** 51501 (2021).

[31] X.-Y. Chen, N.-N. Zhang, W.-T. He, X.-Y. Kong, M.-J. Tao, F.-G. Deng, Q. Ai, and G.-L. Long, Global correlation and local information flows in controllable non-Markovian open quantum dynamics, npj Quantum Inf. **8,** 22 (2022).

[32] A. Soare, H. Ball, D. Hayes, J. Sastrawan, M. C. Jarratt, J. J. McLoughlin, X. Zhen, T. J. Green, and M. J. Biercuk, Experimental noise filtering by quantum control, Nat. Phys. **10,** 825 (2014).

[33] A. Soare, H. Ball, D. Hayes, X. Zhen, M. C. Jarratt, J. Sastrawan, H. Uys, and M. J. Biercuk, Experimental bath engineering for quantitative studies of quantum control, Phys. Rev. A **89,** 042329 (2014).

[34] N. Khaneja, T. Reiss, C. Kehlet, and T. Schulte-Herbrüggen, Optimal control of coupled spin dynamics: Design of NMR pulse sequences by gradient ascent algorithms, J. Magn. Reson. **172,** 296 (2005).

[35] J. Li, X. Yang, X. Peng, and C.-P. Sun, Hybrid Quantum-Classical Approach to Quantum Optimal Control, Phys. Rev. Lett. **118,** 150503 (2017).

[36] I. Buluta and F. Nori, Quantum simulators, Science **326,** 108 (2009).

[37] I. M. Georgescu, S. Ashhab, and F. Nori, Quantum simulation, Rev. Mod. Phys. **86,** 153 (2014).

[38] S. Luo, S. Fu, and H. Song, Quantifying non-Markovianity via correlations, Phys. Rev. A **86,** 044101 (2012).

[39] X.-M. Lu, X. Wang, and C. P. Sun, Quantum Fisher information flow and non-Markovian processes of open systems, Phys. Rev. A **82,** 042103 (2010).

[40] A. Altherr and Y. Yang, Quantum Metrology for Non-Markovian Processes, Phys. Rev. Lett. **127,** 060501 (2021).

[41] J. W. Goodman, *Statistical Optics* (John Wiley & Sons, New York, 2015).

[42] M.-J. Tao, N.-N. Zhang, P.-Y. Wen, F.-G. Deng, Q. Ai, and G.-L. Long, Coherent and incoherent theories for photosynthetic energy transfer, Sci. Bull. **65,** 318 (2020).

[43] See Supplemental Material at http://link.aps.org/supplemental/10.1103/PhysRevLett.129.070502 for the complete description of the theory, experimental details, and numerical simulations, which includes Ref. [44].

[44] J. J. Rissanen, Fisher information and stochastic complexity, IEEE Trans. Inf. Theory **42,** 40 (1996).

[45] E. Knill, R. Laflamme, R. Martinez, and C. H. Tseng, An algorithmic benchmark for quantum information processing, Nature (London) **404,** 368 (2000).

[46] R. Laflamme, D. Cory, C. Negrevergne, and L. Viola, NMR quantum information processing and entanglement, Quantum Inf. Comput. **2,** 166 (2002).

[47] A. Potočnik, A. Bargerbos, F. A. Y. N. Schröder, S. A. Khan, M. C. Collodo, S. Gasparinetti, Y. Salathé, C. Creatore, C. Eichler, H. E. Türeci, A. W. Chin, and A. Wallraff, Studying light-harvesting models with superconducting circuits, Nat. Commun. **9,** 904 (2018).